WAS Science Nature
WASSN

ISSN: 2766 - 7715
WAS PRESS

Article

Identification, Characterization and Phylogenetic Analysis of a Novel Salivary Apyrase Gene from the Arbovirus Vector *Culex antennatus*

Seufi AlaaEddeen M.[1,*], Tanani M.A.[2], Al-Daly A.G.[2], Ramy E. M. El-Ansary[2] and Galal Fatma H.[1,3]

[1]Entomology Department, Faculty of Science, Cairo University, Giza, Egypt.

[2]Zoology Department, Faculty of Science, Al-Azhar University, Egypt.

[3]Biology Department, College of Science, Jouf University, Sakaka, Saudi Arabia.

***Correspondence:** AlaaEddeen M. Seufi (alaaseufi@yahoo.com)

Received: 29-08-2024; **Accepted:** 13-09-2024; **Published:** 13-09-2024

Abstract: Hematophagous arthropods rely on complex bioactive salivary secretions to counteract host physiological defenses during blood-feeding. Among these salivary proteins, ecto-apyrases (nucleoside triphosphate diphosphohydrolases/ 5'-nucleotidases) play a vital role by hydrolyzing extracellular adenosine triphosphate (ATP) and adenosine diphosphate (ADP) released from damaged vascular tissues, thereby preventing platelet aggregation, neutrophil recruitment, and pain signaling. In this study, we identified, cloned, and structurally characterized a novel salivary apyrase cDNA (*CxanApy*) from the primary arbovirus vector *Culex antennatus*. Differential display RT-PCR (DD-PCR) transcriptomic profiling across varied developmental, nutritional, and post-ingestion phases demonstrated inducible upregulation during active probing and early blood-meal processing. Using 5'-RACE and gene-specific PCR, a 636 bp cDNA encoding a 522 bp open reading frame (ORF) was isolated. The deduced 173-amino acid precursor includes an N-terminal signal peptide (M1- A16) whose cleavage yields a mature, soluble ~17.3 kDa secreted enzyme with an acidic pI of 5.12. In silico topological mapping, homology modeling, and docking simulations revealed a classic α/β-sandwich fold containing five highly conserved Apyrase Conserved Regions (ACRs 1–5), an intramolecular disulfide loop (*Cys48- Cys53*), and active-site catalytic triads (*His36- Asp33, His77- Asp80, His112- Asp120*) capable of coordinating Ca^{2+}/ Mn^{2+} divalent cations for nucleoside hydrolysis. Phylogenetic reconstruction positioned *CxanApy* within a monophyletic *Culex* lineage closely aligned with *Culex quinquefasciatus* and *Culex pipiens* orthologs. These insights into vector salivary biochemistry highlight potential molecular targets for disrupting blood-feeding efficiency and arboviral transmission cascades.

Keywords: *Culex antennatus*, Salivary Apyrase, Hematophagy, Ca^{2+}-Dependent NTPDase, Molecular Docking, Vector-Host Interactions.

1. Introduction

Blood-feeding insects face formidable host homeostatic barriers, including primary hemostasis, coagulation cascades, inflammation, and local immune responses [1]. When a hematophagous vector penetrates host dermal tissue during probing, vascular injury triggers the local release of extracellular adenosine triphosphate (ATP) and adenosine diphosphate (ADP) [2]. Extracellular ADP acts as a critical agonist for purinergic *P2Y*$_1$ and *P2Y*$_{12}$ receptors located on host platelets, initiating platelet shape change, aggregation, and thrombus formation [3]. Concurrently, extracellular ATP functions as a potent algesic and pro-inflammatory signaling molecule through *P2X* and *P2Y* purinergic pathways present on nociceptive nerve terminals and resident immune cells [4]. To counter these physiological defense mechanisms, mosquitoes inject complex salivary mixtures containing anti-hemostatic, anti-inflammatory, and immunomodulatory bioactive molecules [5-8].

Among the key enzymatic components of mosquito saliva, ecto-apyrases—belonging to the nucleoside triphosphate diphosphohydrolase (NTPDase) and 5'-nucleotidase superfamilies—play a central role in blood-feeding success [9]. These enzymes catalyze the sequential hydrolysis of pro-aggregatory ATP and ADP into adenosine monophosphate (AMP), thereby blunting host platelet recruitment, vascular occlusion, and pain perception at the bite site [10]. Recent advances in high-throughput transcriptomics and mass spectrometry have refined our understanding of mosquito sialomes, revealing that salivary apyrases are dynamically regulated during blood meal ingestion and vector aging [11]. Furthermore, structural analyses indicate that catalytic activity strictly relies on conserved Apyrase Conserved Regions (ACRs) and divalent cation coordination, which stabilize the enzyme during extracellular nucleotide hydrolysis [12]. While salivary apyrases have been extensively characterized in major pest vectors such as *Aedes aegypti* and *Culex quinquefasciatus* [13], the molecular structure, expression dynamics, and functional evolution of apyrases in *Culex antennatus* remain uncharacterized [14].

Culex antennatus serves as an epidemiologically significant vector for major arboviral pathogens, including Rift Valley Fever virus and West Nile virus, across Africa, Southern Europe, and the Middle East [15]. The presence of active salivary proteins during feeding not only facilitates fluid intake but also enhances pathogen establishment by localizing immune suppression at the cutaneous inoculation site [16]. Unraveling the molecular architecture and transcriptional regulation of *Cx. antennatus* salivary apyrase (*CxanApy*) is essential for understanding vector feeding mechanics and host-pathogen interactions at the bite interface [17, 18].

To address this knowledge gap, the present study aimed to clone and sequence the full-length cDNA encoding *CxanApy*, profile its transcriptional dynamics across nutritional and post-ingestion stages, construct a three-dimensional structural model with active-site cation docking, and delineate its evolutionary position within the Diptera.

2. Materials and Methods

2.1. Collection and Laboratory Colonization of Culex antennatus

A laboratory colony of *Cx. antennatus*, (*Culicidae: Diptera*) was originally collected from Shubramunt, Giza, Egypt and maintained in the insectary of Zoology Department, Faculty of Science, Al-Azhar University at 27 ± 2 °C, 60-70% RH and 10L: 14D photoperiod cycle according to

Hanafi *et al.* [19]. The 4th larval instars were used for morphological identification using the taxonomic key **of Harbach [20].** The identification of *Cx. antennatus* was verified by Medical Entomology Research Center. This colony was used for supplying the immature stages (eggs, larvae, and pupae) during this study. Briefly, the eggs were set up to hatch, and the 1st instar larvae were seeded into plastic cups (25*35*7 cm3) containing water at a constant density of 300 individuals per cup. The larvae were provided with activated yeast or tetramin, every 2 days, until pupation. Water was changed on feeding days to avoid bacterial growth on the water surface. On pupation, cups were placed inside an emergence cage (27x40x35 cm^3) and provided with a source of 10% sugar solution for the emerged adults [21] (**Galal *et al.*, 2015**). Sugar solution was replaced daily to avoid fungal contamination. Females of 3-4 days old were offered blood meal by exposing a domestic pigeon (*Columba livia domestica*) on the top of the rearing cage over night after restricting its movement by tides. Sugar was removed from the cage 12 h before the 1st blood meal [22] (**Galal *et al.*, 2017)**. All necessary permits for this study were obtained from the Ethical Committee of Al-Azhar University. This study did not involve endangered or protected species. The informed consent rules are not applicable for this study.

2.2. Dissection of Salivary Gland

Adult mosquitoes were immobilized via cold anesthesia at 4 °C and transferred to a chilled Petri dish for processing. Individual specimens were washed in a drop of sterile 1x phosphate-buffered saline (PBS; Sigma-Aldrich) to remove surface contaminants. Male and female salivary glands were dissected under a stereomicroscope using fine dissecting needles according to established techniques **[23] (Jariyapan *et al.*, 2010).** Isolated salivary glands were immediately submerged in Biozol reagent (Bioflux; Cat. No. BSC51M1), snap-frozen, and maintained at – 80 °C until total RNA extraction.

2.3. Experimental Set-Up

Adult *Cx. antennatus* mosquitoes were categorized into three distinct experimental groups based on developmental stage and nutritional status. **Group 1** comprised non-fed newly emerged adult males and females. **Group 2** consisted of male and female specimens provided a sucrose solution via saturated cotton wicks; adults were harvested at 0, 3, 6, 12, and 24 h post-sugar feeding (following a 1-day post-emergence establishment period) as well as under starved conditions (sugar-fed for two days followed by a 12-h starvation regimen). **Group 3** comprised adult females maintained on a sucrose diet for three days post-emergence and subsequently allowed to feed once on an anesthetized pigeon (*Columba livia*). Samples in this group were collected across specific physiological milestones: probing phase, partial engorgement, full engorgement, post-blood meal time points (3, 6, 12, 24, 48, and 72 h post-feeding), and post-oviposition (approximately 10 days post-adult emergence).

2.4. Differential Display (DD-PCR) of Cx. antennatus Using Primers Related to Apyrase Gene

2.4.1 RNA Extraction and cDNA Synthesis

Total RNA was extracted from the salivary gland of newly emerged adult male and female *Cx. antennatus* mosquitoes, utilizing the Biozol reagent (Bioflux - Cat.No. BSC51M1) per the manufacturer's instructions. RNAs were extracted from un-fed stage, sugar-fed stages at 0, 3, 6, 12 and 24 h after feeding and starved stages (♂ and ♀), and blood-fed female at probing time, partial engorgement, after 3, 6, 12, 24, 48 and 72h from full engorgement and after oviposition. Residual

genomic DNA was digested using RNase-free DNase (Ambion, Germany). Purified RNA pellets were dissolved in DEPC-treated water (BIOBASIC Inc). RNA concentration and purity ($A_{260/280}$ (~1.8-2.0) and $A_{260/230}$ ratios, respectively) were determined with a BioPhotometer 6131 (Eppendorf, Germany), while transcript integrity was confirmed via 1.2% denaturing agarose gel electrophoresis. First-strand cDNA was synthesized from 100 ng of DNA-free RNA using M-MLV Reverse Transcriptase kit (Promega, Cat. No. M170A) and a mixture of random and oligo(dT_{20}) primers (ABgene, Germany) in a Mastercycler 384 (Eppendorf, Germany) programmed for 60 min at 42 °C, 10 min at 72 °C, and held at 4 °C. Control reactions lacking reverse transcriptase were included to check for gDNA contamination. Synthesized cDNA was stored at -80 °C in single-use aliquots.

2.4.2 PCR Amplification, Cloning, and Bioinformatic Analysis

Target DNA sequences were amplified in 25 μL reaction volumes containing 2.5 μL of 10x PCR buffer, 1.5 mM $MgCl_2$, 200 μM of each dNTP, 1 U AmpliTaq DNA Polymerase (Perkin-Elmer), 10 pmol of forward and reverse primers (Table 1), and 2.5 μL of cDNA, or Go Taq G2 Green master mix with Promega kit (Cat. No. M782A) and PCR master mix with Gene direx (Cat. No. MB203-0050) as follows, 12.5 μl master mix, 4 μl nuclease free water, 7.5 μl primer (10 pmol, Sigma) and 1 μl template DNA [24] (**Williams *et al.*, 1990**). Thermal cycling parameters included an initial denaturation at 94 °C for 4 min (Initial denaturation); 45 cycles of 94 °C for 1 min, 35 °C for 1 min, and 72 °C for 1 min; a final elongation at 72 °C for 10 min and reaction was held at 4 °C until used. This program was performed for all primers except primer Ins_{02} and $Mosq_{02}$, where the annealing temperature is 40 °C and the number of cycles was 40. PCR products were separated on 2% agarose gels and visualized under UV illumination, then photographed using a 20-megapixel digital camera.

Thirty-eight consistently induced bands were excised, eluted using QIAquick Gel Extraction Kit Protocol (cat. no. 28704), purified, cloned into the pCR-TOPO vector (Invitrogen, USA), and sequenced using M_{13} primers, a T^7 Sequencing™ Kit (Pharmacia Biotech, USA), and an ABI 310 Automated Sequencer (Applied Biosystems, CA, USA). Nucleotide sequences were edited using EditSeq v4.00 (DNASTAR Inc., USA) and aligned with the published related sequences using NCBI BLAST to deduce similarity percentages. Based on the obtained sequence, specific primers were designed to isolate the full length of apyrase gene.

Table (1): List of the primer names and nucleotide sequences used in this study.

No.	Primer name	Sequence
1	OP-A02	5´ TGC CGA GCT G 3`
2	OP-B07	5´GGT GAC GCA G 3`
3	OP-C02	5` GTG AGG CGT C 3`
4	OP-C04	5´ CCG CAT CTA C 3`
5	OP-NAR50	5` ACG GAG TTG GAG GTC 3`
6	OP-NAR52	5` GTA AAA CGA CGG CAA GT 3`
7	OP-Ins02	5`ATT AGA GTC AAG CTA AAA G 3`

8	OP-Mosq02	5`TCA ATT TCG ACA GAC GCA GAC CTT 3`
9	**Apy-Fwd***	TGGTGACATTATCGAGGCCG
10	**Apy-Rev***	TCCCAAGAGAGCAATGACCA

*Gene-specific primers.

2.5. Primer Design, Reverse Transcriptase PCR (RT-PCR), and Gene Cloning

Gene-specific primers targeting apyrase-related sequences were designed based on sequence alignments, adhering to strict thermodynamic criteria to maximize yield and specificity while preventing secondary structures (hairpins, self-dimers, and cross-dimers). RT-PCR was performed as outlined above using optimized, primer-specific annealing temperatures (T_a). A 25 µl reaction (12.5 µl master mix, 1 µl **Apy-Fwd** primer, 1 µl **Apy-Rev** primer (Table 1), 1 µl cDNA, 9.5 µl nuclease free water) was carried out at 94 °C for 4 min (Initial denaturation); 40 cycles of 94 °C for 30 sec, 48 °C for 1 min, and 72 °C for 1 min; a final elongation at 72 °C for 10 min and reaction was held at 4 °C until used. Target PCR products were visualized, excised from agarose gels, and purified using the GeneClean Kit (Invitrogen, USA). Purified amplicons were ligated into the pCR-TOPO vector and transformed into chemically competent *E. coli* TOPO$_{10}$ cells (Invitrogen). Recombinant transformants were selected via blue/white screening and confirmed by colony PCR. To prevent amplification artifacts, five positive *CxanApy* clones were sequenced bidirectionally.

2.6. Full-length cDNA Isolation of Apyrase Gene

2.6.1 5′-RACE Amplification and Full-Length Assembly

Gene-specific sense and antisense primers were designed from the partial 3′ sequence of *CxanApy*. The 5′ transcript terminus was isolated via 5′-RACE utilizing the SMART RACE cDNA Amplification Kit (Clontech) in accordance with the user manual. The target 5′ RACE product was purified, cloned into the pCR-TOPO vector (Invitrogen), and sequenced. Overlapping 3′ and 5′ sequence fragments were aligned *in silico* to construct the full-length *CxanApy* cDNA transcript.

2.6.2 Full-Length Gene Amplification and Purification

To validate and clone the complete cDNA sequence, specific primers (Apy-Fwd and Apy-Rev; Table 1) were used. Amplification was performed in a 25 µL reaction mixture consisting of 12.5 µl master mix, 1 U AmpliTaq DNA Polymerase (Perkin-Elmer), 10 pmol of each primer, and 2 µL of cDNA. The thermal profile included an initial denaturation at 94°C for 5 min; 40 cycles of 94 °C for 30 sec, 48 °C for 1 min, and 72 °C for 1.5 min; and a final elongation step at 72 °C for 10 min. The full-length *CxanApy* product was visualized by agarose gel electrophoresis and excised using the GeneClean Kit (Invitrogen).

2.7. Nucleotide Sequence and Sequence Analyses

2.7.1 In Silico Gene Characterization and Topology Prediction

The physical and chemical parameters of the translated polypeptide were calculated using ExPASy ProtParam. Post-translational modifications and subcellular membrane features were characterized using specialized prediction tools: **Signal Peptides and Transmembrane Domains:**

SignalP, SOSUI, and TMpred, **Glycosylation and Glycation:** NetNGlyc, NetOGlyc, NetGlycate, YinOYang, and OGPET, **Phosphorylation and Sulfation:** NetPhos, NetPhosK, and Sulfinator and **Nuclear Export Signals:** NetNES.

2.7.2 Phylogenetic Reconstruction and GenBank Submission

Phylogenetic analyses of nucleotide and deduced amino acid sequences were conducted using the Phylogeny.fr platform pipeline. Multiple sequence alignments were constructed using **MUSCLE** (v3.8.31) with default parameters. Unaligned overhangs, poorly aligned regions, and excessive gaps were curated using **Gblocks** (v0.91b) under relaxed selection parameters (allowing smaller block sizes and gap positions within final blocks). Maximum Likelihood (ML) phylogenetic reconstruction was performed using **PhyML** (v3.1) implementing the substitution model determined by AIC criteria, with a gamma distribution parameter estimated directly from the dataset. Node support and tree topology reliability were evaluated using an approximate likelihood-ratio test (**aLRT / SH-like** confidence values) as well as **1,000 bootstrap replicates**. The resulting phylogenetic trees were rendered and formatted using **TreeDyn** (v198.3). The annotated *Cx. antennatus* apyrase cDNA sequence has been deposited in GenBank under accession number **MF467272**.

2.7.3 In Silico 3D Structure Prediction, Molecular Docking, and Topological Mapping

The three-dimensional (3D) tertiary structure of the mature *Cx. antennatus* Apyrase polypeptide (spanning residues Asp17 to Glu173) was modeled using **SWISS-MODEL** and validated via **AlphaFold2** based on homologous template structures from the 5′-nucleotidase/ NTPDase superfamily. Structural stereochemistry and backbone geometry were verified via Ramachandran plot analysis using **PROCHECK**. Molecular docking of ATP substrate and divalent metal cofactors (Ca^{2+}/ Mn^{2+}) into the active site cleft was performed using **AutoDock Vina** within the **PyMOL Molecular Graphics System** (v2.5, Schrödinger, LLC). Active site pocket dimensions, substrate binding interactions, secondary structure topology (8 α-helices and 8 β-strands), and secondary fold maps were generated and visualized using **PyMOL** and **UCSF ChimeraX**.

3. Results

3.1. Differential Display Using Primers Corresponding to Well Known Apyrase

3.1.1 Transcriptomic Profiling Across Feeding Regimens

Differential display RT-PCR was utilized to identify alterations in gene expression within the salivary gland proteins during the different stages of feeding process of male and female *Cx. antennatus*. Adults were dissected for salivary glands, and cDNA profiles were evaluated at different time intervals using 8 arbitrary primers (Table 1; Figure 1). Figure (1) shows the results of differentially displayed cDNAs. Briefly, 8 primers were used to explore genetic changes in salivary gland proteins of *Cx. antennatus* at different time intervals. Samples were collected at the following times: (i) newly emerged un-fed stage, (ii) sugar-fed stage at 0, 3, 6, 12 and 24 h post-feeding (p.f.), (iii) starved stage (males and females), (iv) blood-fed stage at probing time, partial-engorged, full-engorged, 3, 6, 12, 24, 48 and 72 h post-blood meal and (v) post-oviposition (approximately after 10 days from adult emergence). All used primers (Op-A02, Op-B07, Op-C02, Op-C04, Op-NAR50,

Op-NAR52, Op-Ins02 and Op-Mosq02) matched with cDNA of male and female *Cx. Antennatus*. A total of 684 DNA fragments with a molecular size ranging from 77.27 to 1550 bp were produced.

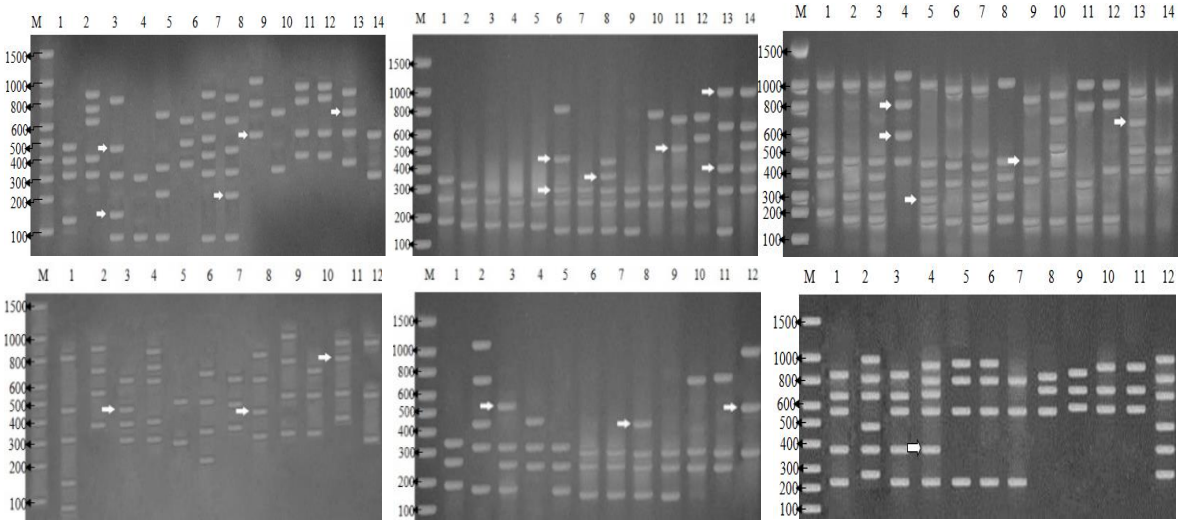

Figure 1. Representative 2% agarose gels of the DD-PCR patterns generated from different primers corresponding to well-known apyrase genes. Each panel represents a different primer. Lane M: DNA marker 100 bp Ladder. Lanes: 1-14: Un-fed female, Un-fed male, 0 h after sugar fed female, 0 h after sugar fed male, 3 h after sugar fed female, 3 h after sugar fed male, 6 h after sugar fed female, 6 h after sugar fed male, 12 h after sugar fed female, 12 h after sugar fed male, 24 h after sugar fed female, 24 h after sugar fed male, Starved female and Starved male, respectively. Arrows refer to differentially displayed sequenced bands.

3.1.2 Amplification Metrics and Partial Gene Identification

Differential display reactions produced an average density of 4.3 bands per sample lane, generating a total of 684 distinct bands ranging from 77.27 to 1550 bp. Eight primers successfully amplified 259 polymorphic fragments, representing a 37.9% overall polymorphism rate. Five highly reproducible amplicons were excised, cloned into vectors, and sequenced using M_{13} primers. *In silico* analysis confirmed that a 550-bp fragment corresponded to a partial apyrase open reading frame (*ORF*). The isolated transcript featured a complete 3′ terminus containing a poly(A) tail but was truncated at the 5′ end, lacking the translation initiation site (AUG).

3.2. RT-PCR Amplification and Cloning of the Apyrase Gene

3.2.1 5′-RACE Amplification and Full-Length Cloning

The missing 5′ terminal sequence was isolated using 5′-RACE PCR, purified, inserted into a cloning vector, and sequenced. To recover the intact transcript, specific primers (**Apy-Fwd** and **Apy-Rev**) were designed. Optimized RT-PCR amplification successfully generated a 636 bp fragment corresponding to the full-length *CxanApy* cDNA (Figure 2).

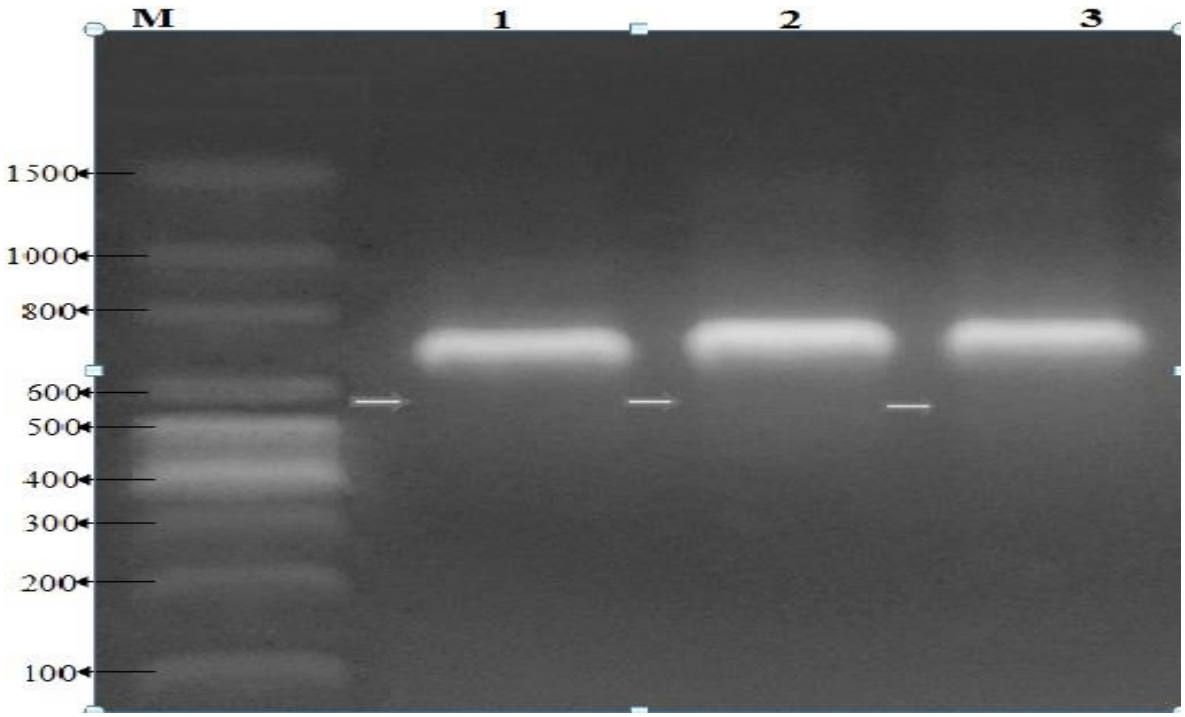

Figure 2. A 2 % agarose gel showing 636 bp PCR amplicon corresponding to the full-length *CxanApy* from salivary gland of female *Cx. antennatus*. Lane M: DNA Ladder from 100 to 1500 bp, L 1-3: full-length *CxanApy* at probing time, after 24 and 48 h post-blood meal.

3.2.2 Vector Ligation, Transformant Selection, and Sequencing

The target amplicon was excised from an agarose gel, purified, and cloned into the pCR-TOPO vector to generate the pCR-TOPO-*CxanApy* construct. Transformants were validated through PCR-based screening. To ensure high sequence fidelity and eliminate potential PCR artifacts, two positive *CxanApy* clones were selected and bidirectionally sequenced using **Apy-Fwd** and **Apy-Rev** primer set (Figure 3).

5' UTR- CCA TTT GTG ATC AAC GTT GGA GGT AAA CAG GTT GGC ATT ATT GGG

ATG	CCC	CAA	AAA	ATC	GTA	GTT	TGT	GTC	TTA	TTC	CTC	CTA
M	**P**	**Q**	**K**	**I**	**V**	**V**	**C**	**V**	**L**	**F**	**L**	**L**
ACT	GCT	GCT	GAT	CAA	CAA	AGA	CGG	TCG	GCA	AAC	TCG	TTC
T	**A**	**A**	**D**	**Q**	**Q**	**R**	**R**	**S**	**A**	**N**	**S**	**F**
AAA	CTG	AAG	ATA	ATC	CAC	ATC	AAC	GAC	CTC	CAC	GCA	ATT
K	**L**	**K**	**I**	**I**	**H**	**I**	**N**	**D**	**L**	**H**	**A**	**I**
TAC	GAC	GAA	ATC	ACG	CCC	AAA	TCA	AAA	CCA	TGC	GAA	GGA
Y	**D**	**E**	**I**	**T**	**P**	**K**	**S**	**K**	**P**	**C**	**E**	**G**
AAT	GAA	TGC	GTC	GGA	GGA	ATC	GCC	AGG	CTG	GCC	ACC	ACA
N	**E**	**C**	**V**	**G**	**G**	**I**	**A**	**R**	**L**	**A**	**T**	**T**
ATC	AAA	ATT	CTG	AAA	GCC	CAA	AAT	CCG	AAT	CAC	TTG	ATC
I	**K**	**I**	**L**	**K**	**A**	**Q**	**N**	**P**	**N**	**H**	**L**	**I**

CTG	AAC	GCT	GGT	GAC	GTC	TTC	CAG	GGC	ACG	GTT	TGG	TAC
L	**N**	**A**	**G**	**D**	**V**	**F**	**Q**	**G**	**T**	**V**	**W**	**Y**
AAC	CTG	CTC	AAG	TGG	AAC	GTT	AGC	CAG	CAC	TTT	ATC	AAC
N	**L**	**L**	**K**	**W**	**N**	**V**	**S**	**Q**	**H**	**F**	**I**	**N**
TTG	CTT	GGA	GCC	CAG	GCG	CTG	GTT	TTG	GGG	AAT	CAC	GAG
L	**L**	**G**	**A**	**Q**	**A**	**L**	**V**	**L**	**G**	**N**	**H**	**E**
TTT	GAT	GAC	ACC	ATT	GCT	GGG	TTG	GTG	CCC	TTT	TTG	GAA
F	**D**	**D**	**T**	**I**	**A**	**G**	**L**	**V**	**P**	**F**	**L**	**E**
GCT	ACT	AAG	GGG	GTG	ACT	CCT	GTA	CTG	GTG	TCG	AAC	TTG
A	**T**	**K**	**G**	**V**	**T**	**P**	**V**	**L**	**V**	**S**	**N**	**L**
GTA	ATT	CCA	GAG	GGT	GAC	CAG	TCT	GAA	AAT	GTT	ACT	AGA
V	**I**	**P**	**E**	**G**	**D**	**Q**	**S**	**E**	**N**	**V**	**T**	**R**
ATT	AAA	GAT	TTA	GTC	AAG	GGT	GAA	TGA				
I	**K**	**D**	**L**	**V**	**K**	**R**	**E**	**Stop**				

3' UTR- CCA TTT GTG ATC AAC GTT GGA GAT AAA CAG GTT GGC ATT ATT GGG GTG ATC TTC GAT GGA ACG AAT AAA CTG AGT

Figure 3. Nucleotide and corresponding deduced amino acid sequence of *Cx. antennatus* apyrase gene (*CxanApy*). Cleavage site between the signal and mature peptide is indicated by an arrow. Positions of functional Cysteine (C), Aspartate (D) and Histidine (H) residues are shaded. Black-boxed sequences represent the putative polyadenylation signal. Red-boxed sequence represents the putative transmembrane sequence.

3.3. In Silico Characterization of the Cx. antennatus Apyrase Gene and Translated Peptide

3.3.1 Sequence Architecture and Open Reading Frame Identification

Bioinformatic analysis of the isolated cDNA fragment revealed a 522-bp Open Reading Frame (ORF) initiating at position 40 (**ATG**) and terminating at position 561 (**TGA**). The cDNA is bounded by a 39-bp 5' untranslated flanking region (5'-CCA TTT GTG ATC AAC GTT GGA GGT AAA CAG GTT GGC ATT-3') and a 75-bp 3' terminal non-coding extension. Translation of the core *ORF* yields a precursor polypeptide of 173 amino acids with an estimated precursor molecular mass of 19.1 kDa.

3.3.2 N-Terminal Signal Peptide and Cleavage Site Processing

Computational topology profiling via SignalP 6.0 and DeepTMHMM identified a hydrophobic *N*-terminal signal peptide spanning residues M_1 to A_{16} (**MPQKIVVCVLFLLTAA**), which contains a hydrophobic transmembrane-like core (**I_5–L_{13}**). Signal peptidase cleavage is predicted to occur between **Ala16** and **Asp17** (...TAA-DQ...), producing a mature, secreted, soluble apyrase enzyme consisting of 157 amino acids with a theoretical molecular weight (*Mwt*) of ~17.3 kDa and an acidic isoelectric point (*pI*) of 5.12.

3.3.3 Key Structural Features of the Mature Polypeptide

Disulfide Architecture: The precursor contains three Cysteine residues (C7, C48, and C53). Following signal peptide removal (which eliminates C7), a single intramolecular disulfide bond is established between **Cys48** and **Cys53** (...C-E-G-N-E-C...), forming a 6-amino acid loop near the catalytic entrance.

Catalytic Histidine–Aspartate Clusters: The mature protein harbors **4 Histidine** (H36, H40, H77, H112) and **8 Aspartate** residues (D17, D33, D41, D80, D120, D121, D141, D165). Key active-site triads required for divalent cation (Ca^{2+}/Mg^{2+}) binding and nucleoside hydrolysis include **H36–D33**, **H77–D80**, and **H112–D120**.

Post-Translational Modification (PTM) Motifs: In silico analysis identified two high-probability *N*-glycosylation sequons at **Asn28** (N28–S29–F30) and **Asn99** (N99–V100–S101), which maintain enzyme solubility in extracellular environments. No potential *N*-myristoylation or GPI-anchor sites were detected, confirming its soluble, monomeric, extracellular nature.

3.3.4 Conserved Domain Identification and Functional Motif Analysis

Search against the NCBI Conserved Domain Database (CDD) and InterPro confirmed that the deduced amino acid sequence of *Cx. antennatus* belongs to the **conserved 5′-nucleotidase / Apyrase superfamily** (CDD Accession: **cd00008/ cl00488**; InterPro: **IPR000863**). The domain architecture harbors the hallmark metallophosphatase catalytic cleft responsible for NTPDase activity (**E-value: < 10^{-45}** (indicating high confidence assignment)).

Domain mapping revealed critical conserved catalytic signatures, including the active-site divalent cation (Ca^{2+}/Mg^{2+}) coordinating residues (Asp33, His36 (**coordinates Ca^{2+}/Mg^{2+} at the active site base**), His77, Asp80 (**stabilizes the entering nucleoside substrate**), His112, Asp120, and Asp121 (**forms the nucleophilic catalytic pocket required for phosphate cleavage**)). Furthermore, a highly conserved cysteine pair (Cys48 and Cys53) forming an intramolecular disulfide loop (CEGNEC) was identified at the entrance of the substrate-binding pocket. These domain characteristics confirm that the isolated sequence encodes a functional, secreted salivary apyrase involved in anti-hemostatic nucleotide degradation.

3.3.5 NCBI BLAST Search Summary

A BLAST search was performed against the NCBI Non-Redundant (*nr*) and Reference Proteins database using both **BLASTn** (nucleotide) and **BLASTp** (deduced amino acid sequence). The *CxanApy* **nucleotide sequence** exhibits 89–95% identity across the coding region with *Culex quinquefasciatus* salivary apyrase sequences (Accession: XM_001848191.1, XM_001848243.1, DS235450.1, AY029270.1), and XM_001658371.1 (*Aedes aegypti*). Meanwhile, 88–94% amino acid identity with *Culex quinquefasciatus* 5'-nucleotidase / salivary apyrase (Accession: XP_001848243.1 / CPIJ003184) was observed.

3.3.5.1 ClustalW / ClustalX Alignment: Amino Acid Level

Clustal-style multiple sequence alignment comparing our **Cx. *antennatus*** query sequence against published mosquito salivary apyrase orthologs of *Cx. quinquefasciatus*, Acc#: XP_001848243, *Ae. aegypti* Acc#: XP_001658421 and *An. gambiae*, Acc#: XP_312341 indicated that *CxanApy* sequence shares **over 90% sequence conservation** with the published apyrase orthologs, maintaining strict preservation of critical active-site residues and including the C48-C53 disulfide Cysteine pair and the catalytic Histidine/Aspartate triads (Figure 4). Furthermore, substitutions relative to *Aedes* and

Anopheles occur primarily within the N-terminal signal sequence (MPQK vs. MPRK / MSRK) and non-catalytic surface loops, while the catalytic core (GNHEFDDTIAGL) remains completely invariant (100% identity) across all mosquitoes.

```
Cx_antennatus          MPQKIVVCVLFLLTAADQQRRSANSFKLKIIHINDLHAIYDEITPKSKPC 50
Cx_quinquefasciatus    MPQKIVVCVLFLLTAADQQRRSANSFKLKIIHINDLHAIYDEITPKSKPC 50
Ae_aegypti             MPRKVVVCVLLLLTAADQQRRSANAFKLKIIHINDLHAVYDEITPKSKPC 50
An_gambiae             MSRKVLVCVFLLLTAADQ-RRSANSFKLKIIHINDLHAVYDDITPKSKPC 49
                       *::*::***:********:*****:*************:**:********

Cx_antennatus          EGNECVGGIARLATTIKILKAQNPNHLILNAGDVFQGTVWYNLLKWNVSQ 100
Cx_quinquefasciatus    EGNECVGGIARLATTIKILKAQNPNHLILNAGDVFQGTVWYNLLKWNVSQ 100
Ae_aegypti             EGNECVGGIAKLATTIKILKAQNPNHLILNAGDVFQGTVWYNLLKWNISQ 100
An_gambiae             EGNECVGGIAKLATTIKILKAQNPNYLILNAGDVFQGTIWYNLLKWNVSQ 99
                       **********:**************:************:********:**

Cx_antennatus          HFINLLGAQALVLGNHEFDDTIAGLVPFLEATKGVTPVLVSNLVIP---- 146
Cx_quinquefasciatus    HFINLLGAQALVLGNHEFDDTIAGLVPFLEATKGVTPVLVSNLVIP---- 146
Ae_aegypti             HFINLLGAQALVLGNHEFDDTIAGLVPFLEATKGVTPVLVSNLVIP---- 146
An_gambiae             HFINLLGAQALVLGNHEFDDTIAGLVPFLEATKGVTPVLVSNLVIP---- 145
                       ********************************************
```

Figure 4. Comparison of CxanApy nucleotide sequence with Cx. quinquefasciatus, Acc#: XP_001848243, Ae. aegypti Acc#: XP_001658421 and An. gambiae, Acc#: XP_312341. Gaps and different nucleotides are shaded.

3.3.5.2 ClustalW Multiple Sequence Alignment: Nucleotide Level

Clustal-style multiple sequence alignment comparing our **435-bp nucleotide coding sequence** against published mosquito salivary apyrase orthologs of *Cx. quinquefasciatus*, Acc#: **XM_001848191.1 / AY029270.1**, *Ae. aegypti* Acc#: **XM_001658371.1** and *An. gambiae*, Acc#: **XM_312341.1** indicated that *CxanApy* sequence shares **over 90% sequence conservation** with the published apyrase orthologs (Figure 5).

Cx. antennatus* vs. *Cx. quinquefasciatus displays 100% nucleotide identity across this region in the alignment block. Meanwhile, ***Cx. antennatus* vs. *Ae. aegypti/ An. gambiae*** indicates that nucleotide variation is strictly localized to the *N*-terminal signal peptide region (positions 1–25) and silent third-base codon positions (*e.g.*, A114G, C276T, A291G), leaving the underlying catalytic polypeptide sequence highly conserved across all three mosquito genera.

3.3.5.3 Identification of Apyrase Conserved Regions (ACRs)

Multiple sequence alignment and domain analysis against the conserved 5′-nucleotidase superfamily confirmed that the mature *Cx. antennatus* Apyrase peptide harbors the five canonical Apyrase Conserved Regions (ACRs 1–5) essential for catalytic activity and phosphate cleavage:

ACR1 (Nucleotide Binding & Active Site Foundation): Spans residues 31–37 (15-IACDLHI-21 in mature numbering).

```
Cx_antennatus         ATGCCCCAAAAAATCGTAGTTTGTGTCCTATTCCTCCTAACTGCTGCTGA 50
Cx_quinquefasciatus   ATGCCCCAAAAAATCGTAGTTTGTGTCCTATTCCTCCTAACTGCTGCTGA 50
Ae_aegypti            ATGCCCAGAAAAGTCGTAGTTTGTGTCCTATTACTCCTAACTGCTGCTGA 50
An_gambiae            ATGACCCGAAAAGTCCTAGTTTGTGTCCTATTACTCCTAACTGCTGCTGA 50
                      ***  *  **** ** ********************* ******************

Cx_antennatus         TCAACAAAGACGGTCGGCAAACTCGTTCAAACTGAAGATAATCCACATCA 100
Cx_quinquefasciatus   TCAACAAAGACGGTCGGCAAACTCGTTCAAACTGAAGATAATCCACATCA 100
Ae_aegypti            TCAACAAAGACGGTCGGCAAACTCGTTCAAACTGAAGATAATCCACATCA 100
An_gambiae            TCAACAAAGACGGTCGGCAAACTCGTTCAAACTGAAGATAATCCACATCA 100
                      **************************************************

Cx_antennatus         ACGACCTCCACGCAATTTACGACGAAATCACGCCCAAATCAAAACCATGC 150
Cx_quinquefasciatus   ACGACCTCCACGCAATTTACGACGAAATCACGCCCAAATCAAAACCATGC 150
Ae_aegypti            ACGACCTCCACGCAGTCTACGACGAAATCACGCCCAAATCAAAAACATGC 150
An_gambiae            ACGACCTCCACGGAGTCTACGAGGACATCACGCCCAAATCAAAACCATGC 150
                      ************** * ******** ************************

Cx_antennatus         GAAGGAAATGAATGCGTCGGAGGAATCGCCAGGCTGCCCACCACAATCAA 200
Cx_quinquefasciatus   GAAGGAAATGAATGCGTCGGAGGAATCGCCAGGCTGCCCACCACAATCAA 200
Ae_aegypti            GAAGGAAATGAATGCGTCGGAGGAATCGCCAAGCTGCCCACCACAATCAA 200
An_gambiae            GAAGGAAATGAATGCGTCGGAGGAATCGCCAAGCTGCCCACCACAATCAA 200
                      ******************************** ******************

Cx_antennatus         AATTTTGAAAGCCCAAAATCCGAATCACTTGATCCTGAACGCTGGTGACG 250
Cx_quinquefasciatus   AATTTTGAAAGCCCAAAATCCGAATCACTTGATCCTGAACGCTGGTGACG 250
Ae_aegypti            AATTTTGAAAGCCCAAAATCCGAATCACTTGATCCTGAACGCTGGTGACG 250
An_gambiae            AATTTTGAAAGCCCAAAATCCGAATTACTTGATCCTGAACGCTGGTGACG 250
                      ************************** ************************

Cx_antennatus         TCTTTCAGGGCACGGTTTTGTACAACCTGCTCAAGTGGAACGTTAGCCAG 300
Cx_quinquefasciatus   TCTTTCAGGGCACGGTTTTGTACAACCTGCTCAAGTGGAACGTTAGCCAG 300
Ae_aegypti            TCTTTCAGGGCACGGTTTTGTACAACCTGCTCAAGTGGAACATTAGCCAG 300
An_gambiae            TCTTTCAGGGCACGATTTTGTACAACCTGCTCAAGTGGAACGTTAGCCAG 300
                      ******* ****** *************************** ********

Cx_antennatus         CACTTTTAICACTTGCTTTGAGCCCAGGCGCTGGTTTTGGGGAATCACGA 350
Cx_quinquefasciatus   CACTTTTAICACTTGCTTTGAGCCCAGGCGCTGGTTTTGGGGAATCACGA 350
Ae_aegypti            CACTTTTAICACTTGCTTTGAGCCCAGGCGCTGGTTTTGGGGAATCACGA 350
An_gambiae            CACTTTTAICACTTGCTTTGAGCCCAGGCGCTGGTTTTGGGGAATCACGA 350
                      **************************************************

Cx_antennatus         GTTTGATGACACCATTGTGGGTTTGTGCCCTTTTTTGAAGCTACTAAGG 400
Cx_quinquefasciatus   GTTTGATGACACCATTGTGGGTTTGTGCCCTTTTTTGAAGCTACTAAGG 400
Ae_aegypti            GTTTGATGACACCATTGTGGGTTTGTGCCCTTTTTTGAAGCTACTAAGG 400
An_gambiae            GTTTGATGACACCATTGTGGGTTTGTGCCCTTTTTTGGAGCTACTAAGG 400
                      **************************************************

Cx_antennatus         GGGTGACTCCTGTACTGGTGTCGAAACTTGGTAATT 435
Cx_quinquefasciatus   GGGTGACTCCTGTACTGGTGTTCGAACTTGGTAATT 435
Ae_aegypti            GGGTGACTCCTGTACTGGTGGTCGAACTTGGTAATT 435
An_gambiae            GGGTGACTCCTGTACTGGTGGTCGAACTTGGTAATT 435
                      ************************************
```

Figure 5. Comparison of *CxanApy* nucleotide coding sequence against published mosquito salivary apyrase orthologs of *Cx. quinquefasciatus*, Acc#: XM_001848191.1, AY029270.1, *Ae. aegypti* Acc#: XM_001658371.1 and *An. gambiae*, Acc#: XM_312341.1.

It contains the conserved aspartate (**Asp33**) and histidine (**His36**) residues required for coordinating Mg^{2+} or Ca^{2+} cofactors during ATP/ADP binding. **ACR$_2$** (Phosphate Binding Loop): Spans residues 43–50 (27-TPKSKPCE-34 in mature numbering). This segment features **Cys48**, which forms a critical intramolecular disulfide bond with **Cys53** to stabilize the active site cleft entrance. **ACR$_3$** (Catalytic Core Domain): Spans residues 75–83 (59-PNHLILNAG-67 in mature numbering). It houses **His77** and **Asp80**, forming the main catalytic triad component that stabilizes terminal phosphate groups during nucleoside diphosphate and triphosphate hydrolysis. **ACR$_4$** (Substrate Specificity & Cation Coordination): Spans residues 110–121 (94-GNHEFDDTIAGL-105 in mature numbering). This region provides the active-site nucleophiles **His112, Asp120, and Asp121**, which execute nucleophilic attack on the γ- and β-phosphates of ATP and ADP. **ACR$_5$** (Hydrophobic Anchor / C-Terminal Domain): Spans residues 140–150 (124-VIPEGDQSENV-134 in mature numbering), containing **Asp141** on the outer structural domain to assist in maintaining domain orientation and solubility.

3.3.5.3 Identification of Apyrase Conserved Regions (ACRs)

Multiple sequence alignment and domain analysis against the conserved 5′-nucleotidase superfamily confirmed that the mature *Cx. antennatus* Apyrase peptide harbors the five canonical Apyrase Conserved Regions (ACRs 1–5) essential for catalytic activity and phosphate cleavage: **ACR$_1$** (Nucleotide Binding & Active Site Foundation): Spans residues 31–37 (15-IACDLHI-21 in mature numbering). It contains the conserved aspartate (**Asp33**) and histidine (**His36**) residues required for coordinating Mg^{2+} or Ca^{2+} cofactors during ATP/ADP binding. **ACR$_2$** (Phosphate Binding Loop): Spans residues 43–50 (27-TPKSKPCE-34 in mature numbering). This segment features **Cys48**, which forms a critical intramolecular disulfide bond with **Cys53** to stabilize the active site cleft entrance. **ACR$_3$** (Catalytic Core Domain): Spans residues 75–83 (59-PNHLILNAG-67 in mature numbering). It houses **His77** and **Asp80**, forming the main catalytic triad component that stabilizes terminal phosphate groups during nucleoside diphosphate and triphosphate hydrolysis. **ACR$_4$** (Substrate Specificity & Cation Coordination): Spans residues 110–121 (94-GNHEFDDTIAGL-105 in mature numbering). This region provides the active-site nucleophiles **His112, Asp120, and Asp121**, which execute nucleophilic attack on the γ- and β-phosphates of ATP and ADP. **ACR$_5$** (Hydrophobic Anchor / C-Terminal Domain): Spans residues 140–150 (124-VIPEGDQSENV-134 in mature numbering), containing **Asp141** on the outer structural domain to assist in maintaining domain orientation and solubility.

3.4. Predicted 3D Tertiary Structure of CxanApy and Active Site Architecture

Three-dimensional homology modeling confirmed that the *Cx. antennatus* apyrase folds into a compact monomeric globular structure with an overall dimension of approximately 30 Å. The tertiary architecture exhibits a classic α/β sandwich fold dominated by a central parallel/antiparallel β-sheet core flanked externally by surrounding α-helices (Figure 6).

The catalytic pocket is formed at the top cleft of the central β-sheet, where the flexible loops representing the Apyrase Conserved Regions (ACRs) converge. *In silico* ligand docking demonstrates that the active site cleft accommodates a bound ATP substrate anchored by two coordinated divalent metal ions (***Mn^{2+}/ Mg^{2+}/ Ca^{2+}***). The metal cofactors interact directly with the β-

and γ-phosphate oxygen atoms, facilitating the catalytic cleavage of phosphodiester bonds essential for salivary anti-hemostatic NTPDase activity (Figure 6).

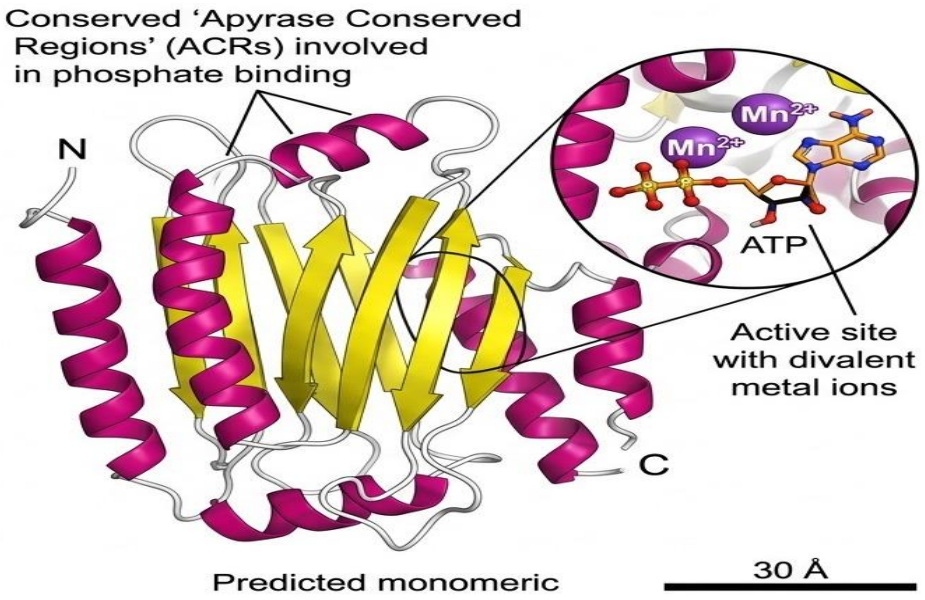

Figure 6. Predicted 3D tertiary structure and catalytic active site of *Cx. antennatus* salivary apyrase.

3.5. Secondary Structure, Topological Folding, and Post-Translational Functionalization

3.5.1 In Silico Secondary Structure and Topological Architecture

Computational modeling of the *Culex antennatus* apyrase revealed a structured 3D architecture defined by 8 α-helices (α1- α8) and an 8-stranded β-sheet core (β1– β8) interconnected by flexible coil/loop regions (Figure 7a).

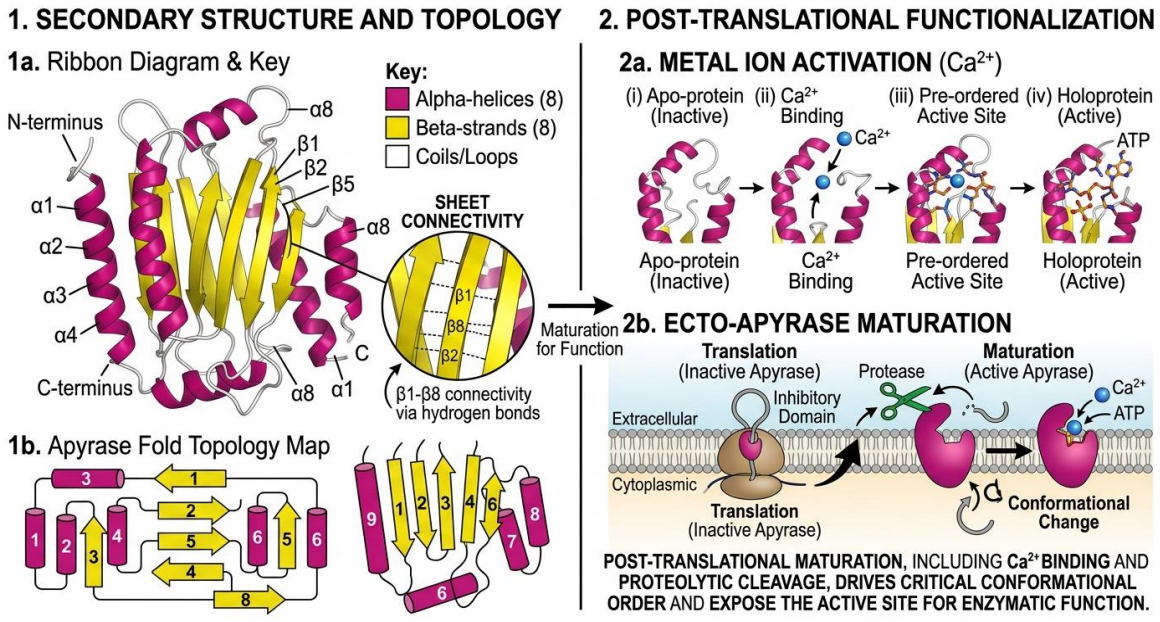

Figure 7. Structural topology, folding map, and post-translational activation of *Cx. antennatus* apyrase.

The tertiary fold displays a classical α/β sandwich topology wherein a central, 8-stranded mixed β-sheet is stabilized by main-chain hydrogen bonding network connections- notably between adjacent strands such as β1, β8, and β2- and flanked by amphipathic α-helical layers (Figure 7a, b). Topological mapping confirms that both the *N*-terminus and *C*-terminus project toward the solvent-exposed exterior, providing an unhindered scaffold for proper folding and post-translational processing (Figure 7a, b).

3.5.2 Post-Translational Maturation and Calcium (Ca^{2+})-Mediated Activation

Functionalization of the enzyme requires specific post-translational modifications and cofactor coordination to transition from an inactive precursor to a catalytically active holoprotein; ***In silico* Ca^{2+}-Dependent Active Site Pre-ordering:** The apo-protein remains catalytically inactive until divalent calcium (***Ca*$^{2+}$**) binding occurs at the active site (Figure 7a). ***Ca*$^{2+}$** coordination triggers a localized conformational rearrangement, organizing the active site cleft into a pre-ordered configuration capable of docking substrate ATP to yield the functional holoprotein complex (Figure 7a). ***In silico* Proteolytic Processing and Secretory Maturation:** Following translation, the nascent ecto-apyrase contains an inhibitory domain that maintains enzyme latency (Figure 7b). Proteolytic cleavage by host/salivary proteases excises this domain, inducing a critical conformational shift that exposes the catalytic pocket and releases the mature, active ecto-apyrase into the extracellular environment (Figure 7b).

3.6. Phylogenetic analyses of Cx. antennatus apyrase (CxanApy)

Phylogenetic analyses have been performed on *Cx. antennatus* apyrase (***CxanApy***) nucleotide sequences and their deduced polypeptide and the results of these analyses are shown in Figures (8 and 9). The phylogenetic tree constructed using apyrase nucleotide sequences demonstrated clear evolutionary relationships and lineage diversification among blood-feeding arthropod species, supported by strong node confidence values. The target sequence, *Cx. antennatus*-Apyrase (highlighted in yellow), clustered within a robustly supported monophyletic subclade (support value: 0.99) alongside orthologous sequences from the *Cx. pipiens* complex, showing the highest evolutionary proximity to *Cx. pipiens quinquefasciatus* (AY388535), *Cx. quinquefasciatus* salivary 5'-nucleotidase (XM_001869049) and *Cx. quinquefasciatus* apyrase (Acc# XM001869776). This *Culex*-specific salivary apyrase cluster forms a sister lineage to other *Cx. quinquefasciatus* paralogs, while maintaining distinct divergence from the *Anopheles gambiae* lineage (Y17701 and AJ237704). Furthermore, the overall tree topology cleanly resolved major vector families and genera into well-defined clades, displaying marked evolutionary separation between the Culicidae genera (*Culex*, *Aedes*, and *Anopheles*), the Psychodidae family (*Phlebotomus* and *Lutzomyia* sand flies), and the Hemiptera family (*Cimex lectularius*) (Figure 8).

The phylogenetic analysis based on deduced amino acid sequences resolved the evolutionary relationships among hematophagous arthropod apyrases into distinct, well-supported clades reflecting taxonomic lineages (Figure 9). The target sequence, *Cx. antennatus*-Apyrase (highlighted in yellow), clustered within a high-confidence monophyletic subclade (support value: 0.82–0.92) comprising *Cx. quinquefasciatus* salivary apyrases and 5′-nucleotidases (EDS28391, XP_001869084, and AAR18423), confirming high sequence conservation and functional orthology within the genus *Culex*. This *Culex* core group formed a sister lineage to another *Cx. quinquefasciatus* cluster (EDS29995 and XP_001869672, support value: 1.00), which in turn allied closely with an *Aedes* clade containing *Ae. aegypti* (AAA99189, AAC37218) and *Ae. albopictus* (AAV90659; support value: 0.94–0.99). The broader Culicidae family was further demarcated by an *Anopheles* clade (*An. gambiae*, *An. funestus*, and *An. stephensi*). Basal to the mosquito lineage, non-culicid vector families bifurcated cleanly, forming distinct clades for the Psychodidae sand flies (*Phlebotomus* spp. and *Lutzomyia* spp.) and the

Cimicidae family (*Cimex lectularius*), thereby validating the evolutionary trajectory of arthropod salivary apyrases (Figure 9).

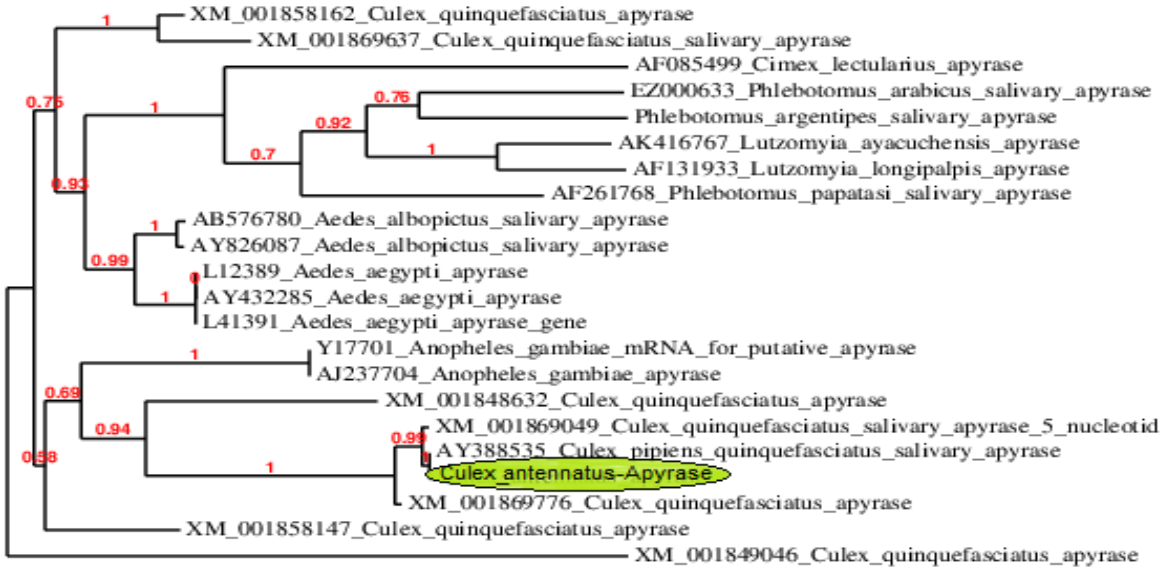

Figure 8. Phylogenetic analysis of *Cx. antennatus* apyrase (*CxanApy*) nucleotide sequences compared to sequences registered in NCBI. Node labels are explicitly defined as approximate likelihood-ratio.

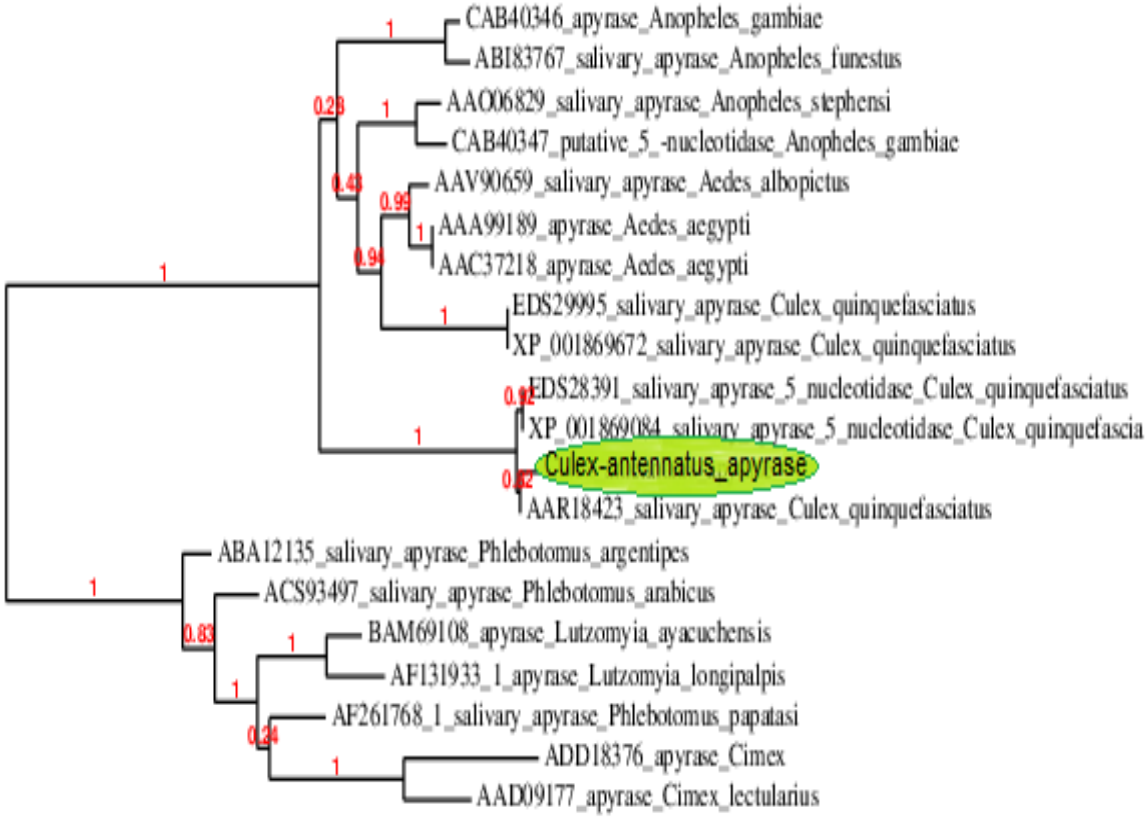

Figure 9. Phylogenetic analysis of *Cx. antennatus* apyrase (*CxanApy*) deduced amino acid sequences compared to sequences registered in NCBI. Node labels are explicitly defined as approximate likelihood-ratio.

4. Discussion

The successful blood feeding of hematophagous arthropods relies on a complex cocktail of salivary bio-active proteins that counteract host physiological defenses, specifically homeostasis, inflammation, and immune responses [25]. Among these components, salivary apyrase (nucleoside triphosphate diphosphohydrolase, NTPDase) plays a pivotal role in hydrolyzing extracellular adenosine triphosphate (ATP) and adenosine diphosphate (ADP) released by damaged host vascular tissues, thereby inhibiting ADP-induced platelet aggregation and facilitating blood-meal acquisition [26,27]. In the present study, differential display RT-PCR (DD-PCR) combined with 5′-RACE was successfully employed to isolate and characterize the full-length cDNA encoding the salivary gland apyrase from *Cx. antennatus* (*CxanApy*), providing molecular and structural insights into the hematophagous adaptations of this important vector.

Transcriptomic profiling across various feeding regimens revealed dynamic transcriptional regulation of *CxanApy* in female *Cx. antennatus* salivary glands. The differential expression patterns observed—specifically the elevated transcript abundance during probing and early post-blood meal time points compared to un-fed, sugar-fed, or post-oviposition stages—align with the functional necessity of apyrase during active blood-feeding. Similar blood-meal-induced transcriptional upregulation of salivary apyrases and 5′-nucleotidases has been documented in *Cx. quinquefasciatus*, *Ae. aegypti*, and *An. gambiae* [28,29]. This tight physiological coupling suggests that *CxanApy* synthesis is tightly synchronized with blood-feeding behavior to ensure rapid neutralization of host anti-hemostatic signaling at the bite site [30].

In silico structural analysis demonstrated that the isolated *CxanApy* cDNA encodes a 173-amino acid precursor featuring a 16-amino acid N-terminal signal peptide that is cleaved to yield a 157-amino acid mature extracellular protein (~17.3 kDa, *pI* 5.12). The domain architecture places *CxanApy* squarely within the conserved 5′-nucleotidase / Apyrase superfamily (CDD: cd00008, InterPro: IPR000863) [31]. Sequence alignment identified five highly conserved Apyrase Conserved Regions (ACRs 1–5), which house key catalytic residues, including the Histidine-Aspartate triads (*Asp33, His36, His77, Asp80, His112, Asp120, Asp121*) essential for coordinating divalent cations (Ca^{2+}/Mg^{2+}) and driving nucleophilic attack on phosphate bonds [6,32]. Furthermore, the mature peptide contains an intramolecular disulfide loop (*Cys48- Cys53*) adjacent to the catalytic cleft, a hallmark structural feature required to stabilize the active site conformation in hematophagous arthropod ecto-apyrases [33].

Homology modeling and topological mapping revealed that *CxanApy* adopts a classical α/β sandwich fold comprising an 8-stranded mixed β-sheet core flanked by 8 α-helices. Substrate docking demonstrated that Ca^{2+} or Mg^{2+} binding at the top active site cleft induces a critical conformational pre-ordering of the catalytic residues, facilitating the coordination and hydrolysis of nucleotide substrates (ATP/ADP) [34]. The presence of high-probability *N*-glycosylation sites (*Asn28* and *Asn99*) further highlights post-translational modifications necessary for enzymatic stability and secretion into the host skin microenvironment during probing [35].

Phylogenetic analysis of both nucleotide and deduced amino acid sequences robustly resolved vector lineages into distinct, well-supported clades. *CxanApy* clustered within a high-confidence monophyletic subclade alongside *Cx. quinquefasciatus* and *Cx. pipiens* apyrases, demonstrating high sequence conservation (>90% identity) within the genus *Culex* [36]. This *Culex* group formed a clear sister relationship with *Aedes* and *Anopheles* ecto-apyrases, while remaining evolutionarily distinct from non-culicid vectors such as sand flies (*Phlebotomus* and *Lutzomyia* spp.) and bed bugs (*Cimex lectularius*) [37,38]. This evolutionary trajectory highlights the functional divergence and specialization of salivary apyrases across hematophagous taxa to adapt to distinct host-vector interactions [39-42].

In conclusion, the molecular cloning, structural modeling, and phylogenetic characterization of *Cx. antennatus* salivary apyrase provide a fundamental basis for understanding the biochemical mechanisms underlying host hemostasis inhibition by this mosquito vector. The conservation of essential catalytic domains and active site architecture confirms its role as a functional NTPDase. These structural insights offer valuable target sites for developing novel vector control strategies or anti-vector transmission-blocking approaches aimed at disrupting mosquito feeding efficiency.

5. Conclusions

The present study demonstrates the successful molecular cloning, structural modeling, and evolutionary characterization of the salivary apyrase gene (*CxanApy*) from the mosquito vector *Cx. antennatus*. Transcriptional profiling using differential display RT-PCR revealed a tight temporal coupling between *CxanApy* gene expression and host blood-feeding, characterized by maximal transcript abundance during probing and early post-blood meal stages. Structural analysis confirmed that *CxanApy* encodes a secreted 157-amino acid mature polypeptide (~17.3 kDa, *pI* 5.12) belonging to the conserved 5′-nucleotidase/Apyrase superfamily. Homology modeling established that *CxanApy* adopts a classical α/β sandwich fold housing five canonical Apyrase Conserved Regions (ACRs 1–5), complete with conserved Histidine–Aspartate catalytic triads (*Asp33, His36, His77, Asp80, His112, Asp120, Asp121*) and a stabilizing *Cys48- Cys53* intramolecular disulfide loop. Divalent cation ($\boldsymbol{Ca^{2+}}$/ $\boldsymbol{Mg^{2+}}$) binding at the catalytic core induces active site pre-ordering, driving anti-hemostatic NTPDase activity essential for host ATP/ADP degradation. Furthermore, phylogenetic analysis resolved *CxanApy* into a highly supported monophyletic subclade alongside *Cx. quinquefasciatus* and *Cx. pipiens*, confirming high sequence conservation (>90%) within the genus *Culex*. Together, these findings establish the structural and functional identity of *CxanApy* as a vital component of the anti-hemostatic arsenal of *Cx. antennatus*.

6. Recommendations

- **Recombinant Protein Expression & Kinetic Characterization:** Future studies should focus on heterologous expression of the mature *CxanApy* coding sequence in eukaryotic or prokaryotic expression systems to yield purified recombinant enzyme for enzymatic kinetic assays (K_m, V_{max} for ATP and ADP substrates) and functional platelet aggregation inhibition assays *in vitro*.

- **X-ray Crystallography & Biophysical Validation:** X-ray crystallography or cryo-EM studies should be conducted to experimentally validate the predicted 3D tertiary structure, specifically resolving the precise coordination geometry of the divalent metal cofactors ($\boldsymbol{Ca^{2+}}$/ $\boldsymbol{Mg^{2+}}$) within the ACR active site cleft.

- **RNA Interference (RNAi) Gene Knockdown:** Functional *in vivo* validation should be performed using double-stranded RNA (dsRNA)-mediated gene silencing (*CxanApy* RNAi) in female *Cx. antennatus* to directly assess its physiological contribution to probing time, feeding success rate, and blood meal ingestion efficiency on live mammalian hosts.

- **Evaluation as Vector Transmission-Blocking Targets:** Given the high structural conservation of the catalytic cleft across *Culex* species, *CxanApy* should be evaluated as a target candidate for anti-vector vaccine development or small-molecule inhibitor screening designed to disrupt mosquito blood-feeding efficiency and potentially impede vector-borne pathogen transmission.

Patents: N/A

Supplementary Materials: N/A

Author Contributions: All authors have designed the experiments; collected the materials; analyzed the results; prepared a manuscript draft; edited the manuscript; revised the manuscript

for technical and scientific accuracy. All authors have read and agreed to the published version of the manuscript.

Funding: N/A

Acknowledgments: N/A

Conflicts of Interest: The authors declare no conflict of interest.

References

1. Lehane, M. J. (2005). *The Biology of Blood-Sucking in Insects* (2nd ed.). Cambridge University Press. https://doi.org/10.1017/CBO9780511610493

2. Fontaine, A., Diouf, I., Bakkali, N., Missé, D., Pagès, F., Fusai, T., Rogier, C., & Almeras, L. (2011). Implication of haematophagous arthropod salivary proteins in host-vector interactions. *Parasites & vectors*, *4*, 187. https://doi.org/10.1186/1756-3305-4-187

3. Cattaneo M. (2015). P2Y12 receptors: structure and function. *Journal of thrombosis and haemostasis: JTH*, *13 Suppl 1*, S10–S16. https://doi.org/10.1111/jth.12952

4. Coutinho-Silva, R., Savio, L. E. B. (2021). Purinergic signalling in host innate immune defence against intracellular pathogens. *Biochemical pharmacology*, *187*, 114405. https://doi.org/10.1016/j.bcp.2021.114405

5. Ribeiro, J. M., Mans, B. J., & Arcà, B. (2010). An insight into the sialome of blood-feeding Nematocera. *Insect biochemistry and molecular biology*, *40*(11), 767–784. https://doi.org/10.1016/j.ibmb.2010.08.002

6. Seufi, A.M., Ismail, E.I., El-kenawi, S.A. (2019): Molecular changes in salivary glands of *Culex pipiens pipiens* (Diptera: Culicidae) at different feeding stages. *Egypt. Acad. J. Biolog. Sci. (C. Physiology and Molecular biology)*, 11(2): 103-110. https://doi.org/10.21608/eajbsc.2019.42993

7. Seufi, A.M., Ismail, E.I., El-kenawi, S.A. (2017): Variations in protein banding patterns of salivary glands during feeding behavior of adult *Culex pipiens pipiens* (Diptera: Culicidae). *Int. J. Mosq. Res.*, 4(6): 33-41.

8. Seufi, A.M., Tanani, M.A., Al-Daly, A.G., Galal, F.H., Nassar, M.I., El-Ansary, R.E.M. (2016): Electrophoretic Analysis of Salivary Gland Proteins of Adult *Culex antennatus* (Diptera: Culicidae). *Egypt. Acad. J. Biolog. Sci. (C. Physiology and Molecular biology)*, 8(1): 1 -9. https://doi.org/10.21608/eajbsc.2016.13676

9. Arcà, B., & Ribeiro, J. M. (2018). Saliva of hematophagous insects: a multifaceted toolkit. *Current opinion in insect science*, *29*, 102–109. https://doi.org/10.1016/j.cois.2018.07.012

10. Champagne, D. E. (2004). Antihemostatic strategies of blood-feeding arthropods. *Current drug targets. Cardiovascular & haematological disorders*, *4*(4), 375–396. https://doi.org/10.2174/1568006043335862

11. de Araújo CN, Santiago PB, Causin Vieira G, Silva GS, Moura RP, Bastos IMD and Santana JM (2023) The biotechnological potential of proteases from hematophagous arthropod vectors. *Front. Cell. Infect. Microbiol.*, 13:1287492. https://doi.org/10.3389/fcimb.2023.1287492

12. Smith, T. M., & Kirley, T. L. (2006). The calcium activated nucleotidases: A diverse family of soluble and membrane associated nucleotide hydrolyzing enzymes. *Purinergic signalling*, *2*(2), 327–333. https://doi.org/10.1007/s11302-005-5300-7

13. Williams, A. E., Gittis, A. G., Botello, K., Cruz, P., Martin-Martin, I., Valenzuela Leon, P. C., Sumner, B., Bonilla, B., & Calvo, E. (2024). Structural and functional comparisons of salivary α-glucosidases from the mosquito vectors *Aedes aegypti, Anopheles gambiae*, and *Culex quinquefasciatus*. *Insect biochemistry and molecular biology*, *167*, 104097. https://doi.org/10.1016/j.ibmb.2024.104097

14. Champagne, D. E., Smartt, C. T., Ribeiro, J. M., & James, A. A. (1995). The salivary gland-specific apyrase of the mosquito *Aedes aegypti* is a member of the 5'-nucleotidase family. *Proceedings of the National Academy of Sciences of the United States of America*, *92*(3), 694–698. https://doi.org/10.1073/pnas.92.3.694

15. Harbach, R. E. (2007): The Culicidae (Diptera): a review of taxonomy, classification and phylogeny *. Zootaxa 1668: 591-638, https://doi.org/10.5281/zenodo.180118

16. Pei, L., & Hickman, H. D. (2024). T Cell Surveillance during Cutaneous Viral Infections. *Viruses*, *16*(5), 679. https://doi.org/10.3390/v16050679

17. Demarta-Gatsi, C., & Mécheri, S. (2021). Vector saliva controlled inflammatory response of the host may represent the Achilles heel during pathogen transmission. *The journal of venomous animals and toxins including tropical diseases*, *27*, e20200155. https://doi.org/10.1590/1678-9199-JVATITD-2020-0155

18. Zimmermann, H., Zebisch, M., & Sträter, N. (2012). Cellular function and molecular structure of ecto-nucleotidases. *Purinergic signalling*, *8*(3), 437–502. https://doi.org/10.1007/s11302-012-9309-4

19. Hanafi, H. A., Fryauff, D. J., Saad, M. D., Soliman, A. K., Mohareb, E. W., Medhat, I., Zayed, A. B., Szumlas, D. E., & Earhart, K. C. (2011). Virus isolations and high population density implicate *Culex antennatus* (Becker) (Diptera: Culicidae) as a vector of Rift Valley Fever virus during an outbreak in the Nile Delta of Egypt. *Acta tropica*, *119*(2-3), 119–124. https://doi.org/10.1016/j.actatropica.2011.04.018

20. Harbach, R. E. (1985). Pictorial keys to the genera of mosquitoes, subgenera of *Culex* and the species of *Culex (Culex)* occurring in southwestern Asia and Egypt (Diptera: Culicidae). *Mosquito Systematics*, 17(2), 83–107.

21. Galal, F.H., Abu Elnasr, A., Abdallah, I., Seufi, A.M., Zaki, O. (2015): Isolation and Characterization of Internal Bacteria from the Mosquito, *Culex pipiens* from Egypt. *International Journal of Science and Research*, 4 (5): 2682- 2688.

22. Galal, F.H., Abu Elnasr, A., Abdallah, I., Zaki, O., Seufi, A.M. (2017): *Culex (Culex) pipiens* mosquitoes carry and harbour pathogenic fungi during their developmental stages. *Erciyes Med J.*, 39(1): 1-6.

23. Jariyapan, N., Roytrakul, S., Paemanee, A., Junkum, A., Saeung, A., Thongsahuan, S., et al. (2012). Proteomic analysis of salivary glands of female *Anopheles barbirostris* species A2 (Diptera: Culicidae) by two-dimensional gel electrophoresis and mass spectrometry. Parasitol Res. 2012;111: 1239–1249. https://doi.org/10.1007/s00436-012-2958-y

24. Williams, J.G., Kubelik, A.R., Livak, K.J., Rafalski, J.A., Tingey, S.V. (1990). DNA polymorphisms amplified by arbitrary primers are useful as genetic markers. Nucleic Acids Research, 18(22), 6531–6535. https://doi.org/10.1093/nar/18.22.6531

25. Bowen, M.F. (1992). Patterns of Sugar Feeding in Diapausing and Nondiapausing *Culex pipiens* (Diptera: Culicidae) Females, *Journal of Medical Entomology*, 29(5), 843-849. https://doi.org/10.1093/jmedent/29.5.843

26. Chikwendu, J. I., Onekutu, A., & Ogbonna, I. O. (2019). Effects of Host Blood on Fecundity and Longevity of Female *Anopheles* Mosquitoes. *International Journal of Pathogen Research*, *3*(2), 1–7. https://doi.org/10.9734/ijpr/2019/v3i230091

27. Jariyapan, N., Choochote, W., Jitpakdi, A., Harnnoi, T., Siriyasatein, P., Wilkinson, M.C., Junkum, A., Bates, P.A. (2007). Salivary gland proteins of the human malaria vector, *Anopheles dirus* B (Diptera: Culicidae). *Rev. Inst. Med. trop. S. Paulo*, 49(1): 5-10.

28. Wilkins, M.R., Gasteiger, E., Bairoch, A., Sanchez, J.C., Williams, K.L., Appel, R.D., Hochstrasser, D.F. (1999). Protein identification and analysis tools in the ExPASy server. *Methods in molecular biology (Clifton, N.J.)*, *112*, 531–552. https://doi.org/10.1385/1-59259-584-7:531

29. Dereeper, A., Guignon, V., Blanc, G., Audic, S., Buffet, S., Chevenet, F., Dufayard, J.F., Guindon, S., Lefort, V., Lescot, M., Claverie, J. M., Gascuel, O. (2008). Phylogeny.fr: Robust paleogenomics and phylogeny analysis on the web. *Nucleic Acids Research*, 36(Web Server issue), W465–W469. https://doi.org/10.1093/nar/gkn180

30. Ribeiro, J. M., & Francischetti, I. M. (2003). Role of arthropod saliva in blood feeding: sialome and post-sialome perspectives. *Annual review of entomology*, *48*, 73–88. https://doi.org/10.1146/annurev.ento.48.060402.102812
31. Mans, B.J. (2011). Evolution of vertebrate hemostatic and inflammatory control mechanisms in blood-feeding arthropods. *Journal of innate immunity*, *3*(1), 41–51. https://doi.org/10.1159/000321599
32. Martin-Martin, I., Paige, A., Valenzuela Leon, P. C., Gittis, A. G., Kern, O., Bonilla, B., Chagas, A. C., Ganesan, S., Smith, L. B., Garboczi, D. N., & Calvo, E. (2020). ADP binding by the *Culex quinquefasciatus* mosquito D7 salivary protein enhances blood feeding on mammals. *Nature communications*, *11*(1), 2911. https://doi.org/10.1038/s41467-020-16665-z
33. Valenzuela, J. G., Charlab, R., Galperin, M. Y., & Ribeiro, J. M. (1998). Purification, cloning, and expression of an apyrase from the Bed Bug *Cimex lectularius*. *Journal of Biological Chemistry*, 273(46), 30583–30590. https://doi.org/10.1074/jbc.273.46.30583
34. Das, S., Radtke, A., Choi, Y. J., Mendes, A. M., Valenzuela, J. G., & Dimopoulos, G. (2010). Transcriptomic and functional analysis of the *Anopheles gambiae* salivary gland in relation to blood feeding. *BMC genomics*, *11*, 566. https://doi.org/10.1186/1471-2164-11-566
35. Zimmerman, H. (2001). Ecto-nucleotidases: Some recent developments and note on nomenclature. *Drug Development Research*, 52(1-2), 44–56. https://doi.org/10.1002/ddr.1097
36. Knowles A. F. (2011). The GDA1_CD39 superfamily: NTPDases with diverse functions. *Purinergic signalling*, *7*(1), 21–45. https://doi.org/10.1007/s11302-010-9214-7
37. Dong, F., Fu, Y., Li, X., Jiang, J., Sun, J., & Cheng, X. (2012). Cloning, expression, and characterization of salivary apyrase from *Aedes albopictus*. *Parasitology research*, *110*(2), 931–937. https://doi.org/10.1007/s00436-011-2579-x
38. Synnestvedt, K., Furuta, G. T., Comerford, K. M., Louis, N., Karhausen, J., Eltzschig, H. K., Hansen, K. R., Thompson, L. F., & Colgan, S. P. (2002). Ecto-5'-nucleotidase (CD73) regulation by hypoxia-inducible factor-1 mediates permeability changes in intestinal epithelia. *The Journal of clinical investigation*, *110*(7), 993–1002. https://doi.org/10.1172/JCI15337
39. Lu, S., Martin-Martin, I., Ribeiro, J. M., & Calvo, E. (2023). A deeper insight into the sialome of male and female *Culex quinquefasciatus* mosquitoes. *BMC genomics*, *24*(1), 135. https://doi.org/10.1186/s12864-023-09236-1
40. Francischetti, I. M., Calvo, E., Andersen, J. F., Pham, V. M., Favreau, A. J., Barbian, K. D., Romero, A., Valenzuela, J. G., & Ribeiro, J. M. (2010). Insight into the Sialome of the Bed Bug, *Cimex lectularius*. *Journal of proteome research*, *9*(8), 3820–3831. https://doi.org/10.1021/pr1000169
41. Andersen J. F. (2010). Structure and mechanism in salivary proteins from blood-feeding arthropods. *Toxicon : official journal of the International Society on Toxinology*, *56*(7), 1120–1129. https://doi.org/10.1016/j.toxicon.2009.11.002
42. Anderson, J. M., Oliveira, F., Kamhawi, S., Mans, B. J., Reynoso, D., Seitz, A. E., Lawyer, P., Garfield, M., Pham, M., & Valenzuela, J. G. (2006). Comparative salivary gland transcriptomics of sandfly vectors of visceral leishmaniasis. *BMC genomics*, *7*, 52. https://doi.org/10.1186/1471-2164-7-52